Journal of Power Sources 244 (2013) 581–585

Contents lists available at SciVerse ScienceDirect

Journal of Power Sources

journal homepage: www.elsevier.com/locate/jpowsour

Short communication

Crystal and local structure studies of $LiFe_{0.48}Mn_{0.48}Mg_{0.04}PO_4$ cathode material for lithium rechargeable batteries

Donghyuk Jang, Kowsalya Palanisamy, Jeongbae Yoon, Yunok Kim, Won-Sub Yoon*

Department of Energy Science, Sungkyunkwan University, Suwon 440-746, Republic of Korea

HIGHLIGHTS

- ► Mg^{2+} substitution causes smaller local structure distortion and disorder during lithium extraction.
- ► Formation of Pseudo one phase reaction favors the lithium ion insertion and structural stability of $LiFe_{0.48}Mn_{0.48}Mg_{0.04}PO_4$.
- ► The smaller lattice mismatch achieved by cation substitution of Mg^{2+} ion in $LiFe_{0.48}Mn_{0.48}Mg_{0.04}PO_4$ system.

ARTICLE INFO

Article history:
Received 21 November 2012
Received in revised form
8 January 2013
Accepted 17 January 2013
Available online 26 January 2013

Keywords:
Lithium-ion battery
Olivine structure cathode
Pseudo one phase reaction
X-ray absorption near edge structure
Extended X-ray absorption fine structure

ABSTRACT

Synchrotron based *in situ* X-ray absorption spectroscopy (XAS) and X-ray diffraction (XRD) techniques are used to investigate changes in the electronic and local structure of $LiFe_{0.48}Mn_{0.48}Mg_{0.04}PO_4$ olivine type cathode material during charge. The Fe and Mn K-edge XANES results show that the major charge compensation is achieved by the oxidation of Fe^{2+} ions at lower potential plateau (~3.5 V) and the oxidation of Mn^{2+} ions at higher potential plateau (~4.1 V). In Fe K-edge EXAFS results, the increase in Fe–O peak intensity during charge indicates the decrease in the degree of structural disorder around Fe ions. Pseudo one phase reaction is observed during charge, which is consistent with the local structural behavior around Fe ions. Trace amount of Mg^{2+} ion decreases the lattice misfit at the phase boundary during Li extraction. The smaller lattice mismatch near the phase boundary facilitates the conversion of one phase to another resulting in less polarization and better rate capability of electrode.

1. Introduction

Lithium metal phosphates ($LiMPO_4$) with ordered olivine structure have been spotlighted as promising cathode materials for lithium rechargeable batteries. The strong P–O bond in orthorhombic lattice makes the olivine structure reasonably more stable than layered and spinel type material. The practical capacity of olivine $LiFePO_4$ cathode material is close to its theoretical value (168 $mAhg^{-1}$). Structural similarity between charged and discharged states of iron phosphate structure not only possesses a good cycle life but also shows excellent safety characteristics when the battery is fully charged. In recent years, there is an increasing interest in olivine structured materials such as $LiMnPO_4$, $LiNiPO_4$ and $LiCoPO_4$ due to their higher chemical potentials compared to $LiFePO_4$. Among the above mentioned materials, structural stability and electrochemical performance of $LiMnPO_4$ match with those of $LiFePO_4$ [1–8].

Crystal structure of $LiMPO_4$ has an orthorhombic unit cell ($\sim D_{2h}^{16}$–$Pmnb$), which accommodates four units of $LiMPO_4$. In phospho olivine compounds, lithium and transition metal ions occupy the 4a and 4c octahedral sites and the oxygen ions are arranged in hexagonal close packed structure. Metal atoms occupy the zigzag chain of corner-shared octahedra running parallel to *c* axis in the alternate *a*–*c* planes. These chains are bridged by corner and edge-shared (PO_4^{3-}) polyanions to form a host structure with a strong three dimensional bonding. Li ions in olivine structure form LiO_6 octahedra which share the corners along *b* axis. These corner-sharing octahedra are separated by vacant tetrahedral and no atom separates Li ion in adjacent site along this direction to screen the electrostatic interaction. Hence, the movement of Li ion is correlated in one-dimensional channel [1,8].

Several hypotheses state that $LiMnPO_4$ material undergoes poor lithium diffusion kinetics due to lower ionic and electronic conductivity and that Jahn–Teller distortion of Mn^{3+} ions and large volume changes between $LiMnPO_4$ and $MnPO_4$ cause large interface strain [6]. On the other hand, $LiMnPO_4$ has higher energy density than $LiFePO_4$ due to its higher chemical potential of

* Corresponding author. Tel.: +82 31 299 6276; fax: +82 31 299 4279.
E-mail address: wsyoon@skku.edu (W.-S. Yoon).

0378-7753/$ – see front matter © 2013 Elsevier B.V. All rights reserved.
http://dx.doi.org/10.1016/j.jpowsour.2013.01.108

Mn^{2+}/Mn^{3+} (4.1 V) redox couple [9]. To overcome the limitations of individual metal phosphate, multi component systems have been proposed, where transition metal ions are combined in an effective way to form a homogenous solid solution phase [1,2,10]. $LiFe_{1-y}Mn_yPO_4$ is considered as one of the most promising binary cathode materials because of its favorable operating voltages between 3.5 and 4.2 V. Yamada et al. reported that $Li(Mn_yFe_{1-y})PO_4$ materials show better kinetic and utilization properties than pure $LiMnPO_4$ electrode material [7].

Divalent cation substitution such as Mg^{2+}, Zn^{2+}, Cu^{2+}, Ni^{2+}, and Co^{2+} in the metal site significantly improves the electronic conductivity and mobility of Li ions in $LiMPO_4$ material [6,11,12]. Hence, clear understanding of the role of cation substitution in multi-component olivine system is crucial for the advancement of cathode material. Here, we report the bulk and local structure behavior of $LiFe_{0.48}Mn_{0.48}Mg_{0.04}PO_4$ during electrochemical extraction of Li-ions by using synchrotron based X-ray absorption and diffraction techniques.

2. Experimental

$LiFe_{0.48}Mn_{0.48}Mg_{0.04}PO_4$ electrodes were provided by UMICORE. For the *in situ* XRD and XAS test, the cathodes were incorporated into *in situ* cells with a metallic Li foil negative electrode and a Celgard separator. The electrolytes used were commercially available 1 M $LiPF_6$ in a 1:1 EC: DMC solvent. XAS measurements were performed in transmission mode at beamline 8C at Pohang Light Source (PLS-II) using a Si (111) double-crystal monochromator detuned to 80% of its original intensity in order to eliminate the high order harmonics. The storage ring was operated with electron energy of 2.5 GeV and a current between 80 and 120 mA. Reference spectrum of each element was simultaneously collected with the corresponding spectrum of the *in situ* cells using Mn and Fe reference foils. The *in situ* XRD patterns were collected at beamline 1D using a Mar 345-image plate detector with the wavelength of 1.0331 Å. For easy comparison, 2θ of all XRD patterns were recalculated and converted to the corresponding angles for $k = 1.54$ Å (Cu-Kα radiation).

EXAFS data analysis was carried out using standard procedures as described in elsewhere [13]. The measured absorption spectrum below the pre-edge region was fitted to a straight line. The background contribution above the post-edge region, $\mu_0(E)$ was fitted to a fourth order polynomial (cubic spline). The fitted polynomials were extrapolated through the total energy region and subtracted from the total absorption spectra. The background subtracted absorption spectra were normalized for the above energy region $\chi(E) = \{(\mu(E) - \mu_0(E)\}/\mu_0(E)$. The normalized $\chi(E)$ spectra were converted to $\chi(k)$ in k space, where $k = [8\pi^2 m(E - E_o)/h^2]^{1/2}$. The $\chi(k)$ spectra were k^3-weighted to magnify the small signal in the higher k space. The normalized k^3-weighted EXAFS spectra, $k^3\chi(k)$, were Fourier transformed (FT) in k space with integration limits of 3.0–11.0 Å^{-1} for Mn and Fe in order to show the contribution of each bond pair. The experimental Fourier fitted $k^3\chi(k)$ spectra were obtained from the inverse transformation with the hanging window function in k space range between 1.0 and 3.0 Å.

3. Results and discussion

First charge profile during *in situ* XAS characterization of $LiFe_{0.48}Mn_{0.48}Mg_{0.04}PO_4$ cathode is shown in Fig. 1. Two distinct voltage plateaus corresponding to the electrochemical reaction of Fe and Mn ions were observed. First voltage plateau corresponds to redox potential of Fe^{2+}/Fe^{3+} (~3.5 V) and second voltage plateau corresponds to redox potential of Mn^{2+}/Mn^{3+} (~4.1 V). This result

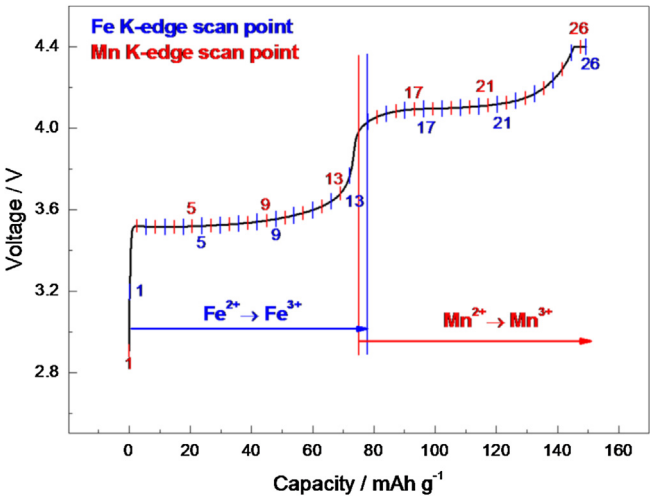

Fig. 1. First charge curves of $LiFe_{0.48}Mn_{0.48}Mg_{0.04}PO_4$ electrode.

is in good agreement with previous results of $Li_{1-x}Mn_{0.5}Fe_{0.5}PO_4$ cathode material [1,4].

Fig. 2(a) and (b) represent *in situ* Fe and Mn K-edge X-ray absorption near edge (XANES) spectra of $LiFe_{0.48}Mn_{0.48}Mg_{0.04}PO_4$

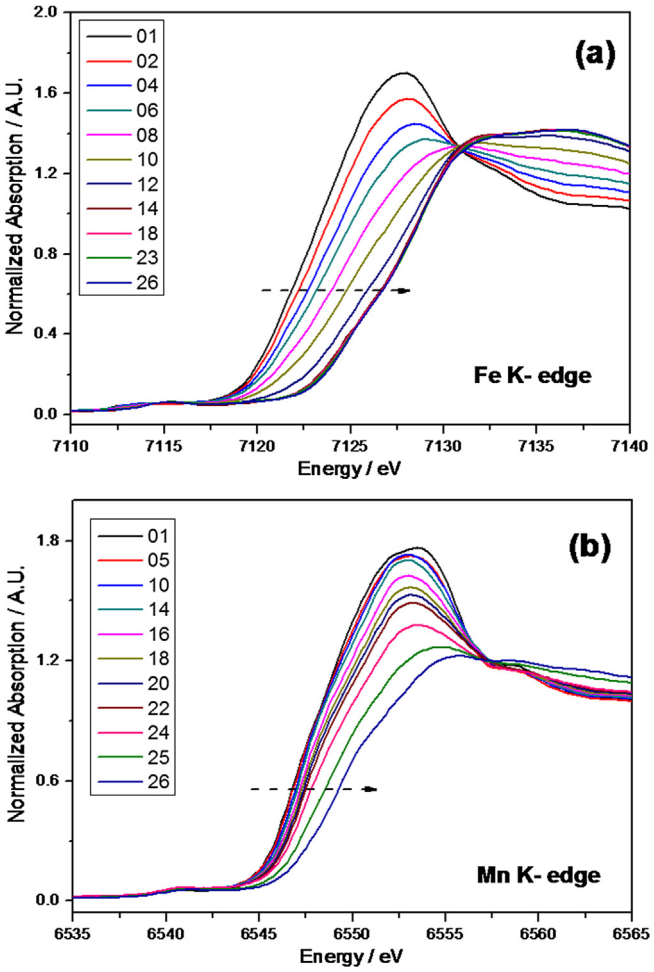

Fig. 2. The normalized *in situ* XANES spectra for (a) Fe and (b) Mn K-edges during first charge.

cathode during charge. This is used to determine the valence state of the selected type of atom and local symmetry of its unoccupied orbital. The metal K-edge XANES spectra originates from symmetry-allowed transitions of 1s core electron of the absorbing element to the excited vacant bound states of proper symmetry in element orbital. This helps in finding out the charge compensation mechanism of the voltage plateaus around 3.5 and 4.1 V as mentioned in the first charge profile curve. XANES spectra clearly specify the appearance of edge shift toward high energy of Fe and Mn region during charge. In Fe K-edge spectra from Fig. 2(a), shift in main peak toward high energy is observed due to a change in valence state of Fe ion in the sample. This means that 1s electron of Fe (III) compound is more strongly bonded to Fe nucleus than Fe (II) compound [13–15]. On the other hand, from Fig. 2(b), there is no strong shift in main peak of Mn K-edge spectrum in its energy level. This indicates that the charge compensation mainly occurs first on Fe ion and then on Mn ion. This is achieved by the oxidation of Fe^{2+} in lower voltage region (~3.5 V) and oxidation of Mn^{2+} in higher voltage region (~4.1 V). The energy position and shape of these edges are very similar to$Li_{1-x}Mn_{0.5}Fe_{0.5}PO_4$ cathode material [4].

Extended X-ray absorption fine structure (EXAFS) is sensitive to atomic species of neighboring atom and provides information about local structure or locally arranged atoms (coordination number, bond length, etc.,) surrounded by interesting atom. Fig. 3(a) and (b) represent Fourier transforms of Fe and Mn K-edge EXAFS spectra. Local arrangement of atoms surrounding Fe and Mn ions in $LiFe_{0.48}Mn_{0.48}Mg_{0.04}PO_4$ during lithium extraction is investigated by EXAFS analysis. The first two strong peaks at ~1.6 and 2.6 Å in Fe and Mn K-edge EXAFS spectra indicate Fe–O and Mn–O interactions in the octahedral environment and Fe–P and Mn–P interactions in tetrahedral environment. The intensity of Fe–O and Mn–O peaks depends on the geometry around the interesting atom. Fe–O peak is broader and lower in amplitude in the beginning and sharpening of peak and increase in amplitude were observed as lithium gets extracted (Fig. 3(a)). This increase in Fe–O peak intensity during charge specifies decrease in degree of structural disorder around Fe atom. Decrease in structural disorder in turn favors the lithium ion diffusivity and the structural stability of olivine material [7,9,16].

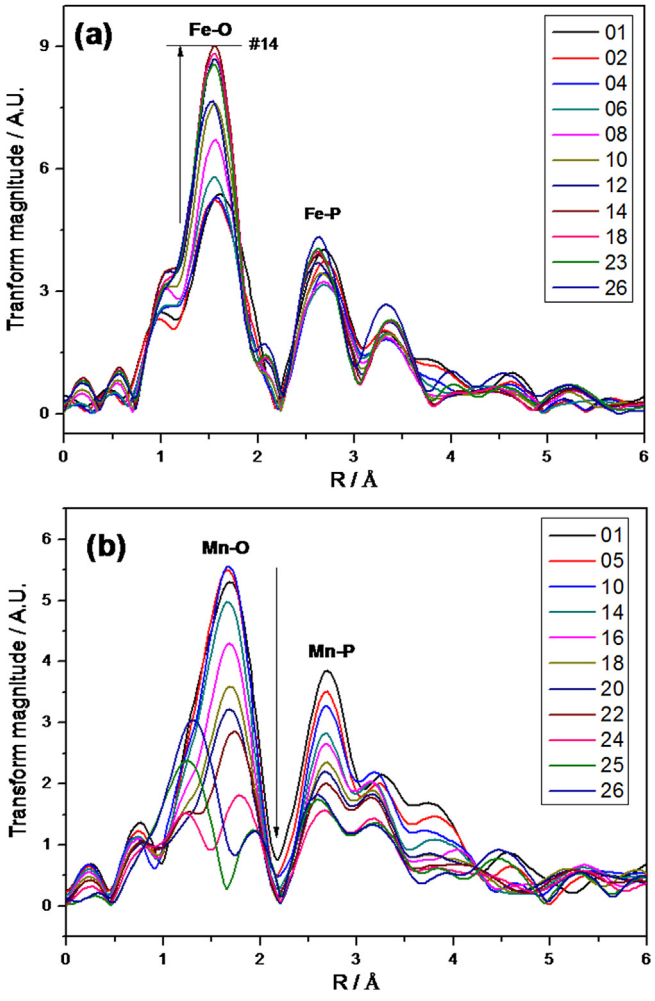

Fig. 3. Selected k^3-weighted Fourier transform magnitudes of the EXAFS spectra of $LiFe_{0.48}Mn_{0.48}Mg_{0.04}PO_4$ at (a) Fe and (b) Mn K-edge during first charge.

By considering the local arrangement of atoms around Mn ion, amplitude of Mn–O peak upon charging decreases significantly compared to Li ($Mn_yFe_{1-y}PO_4$) compound [3,15]. The peak height is related to backscattering of photoelectron by the coordinating atoms. When the distance between absorber atom and coordinating atoms is not uniform, related peak shows a broadening effect and also shows a noticeable decrease in the peak height due to interference between real and imaginary parts of the spectrum. During lithium extraction, oxidation of Mn causes local lattice distortion due to a strong electron–lattice interaction (Jahn–Teller effect). This is well observed from decrease in intensity of Mn–O peak due to Jahn–Teller active Mn^{3+} ion. The Fe and Mn K-edge EXAFS spectra have revealed that the variation in the local structure of Fe and Mn ion shows different tendency toward arrangement of surrounding atoms upon lithium extraction. It is known that the pure $LiFePO_4$ material undergoes two phase reaction. However, Fe^{2+}/Fe^{3+} redox reaction undergoes pseudo one phase reaction when manganese ions coexist in octahedral 4c site and Mn^{2+}/Mn^{3+} redox reaction undergoes first order phase transition between Jahn–Teller active Mn^{3+} phase and Jahn–Teller inactive Mn^{2+} phase [4,5,7]. Recently, Bramnik et al. studied the two phase reactions during lithium extraction in $Li_{1-x}Fe_{0.4}Mn_{0.6}PO_4$ material using high resolution synchrotron *in situ* XRD study [2]. Nam et al. suggested that an intermediate solid solution domain exist in the region where Fe^{2+}/Fe^{3+} electrochemical reaction is replaced by Mn^{2+}/Mn^{3+} in the composition range of ($\sim 0.4 \leq x \leq \sim 0.5$) in carbon coated $Li_{1-x}Mn_{0.5}Fe_{0.5}PO_4$ [4].

The phase changes occurring in $LiFe_{0.48}Mn_{0.48}Mg_{0.04}PO_4$ material in the two theta range around 15–42° (*Pnma* space group) were studied by using *in situ* XRD technique. The structure marked as *phase 1* before charge shows similar olivine phase of uncharged $LiFePO_4$ which is shown in Fig. 4. Upon charging, the reflection from *phase 2* shifts continuously toward the higher angle leading to the formation of pseudo one phase reaction. This follows the first plateau region around 3.5 V unlike previously reported XRD results of $Li(Fe_{1-y}Mn_y)PO_4$ system. It is interesting to note that the small amount of Mg doping changes the structural behavior of $Li(Fe_{1-y}Mn_y)PO_4$ system from clear two phase reactions to pseudo one phase reaction mitigating lattice misfit between two phases during electrochemical cycling. This phase change occurring during charge is consistent with local structure changes from EAXFS analysis. Lattice parameter of cation substituted $LiFe_{0.48}Mn_{0.48}Mg_{0.04}PO_4$ material is calculated by using least square fitting as shown in Fig. 5. The value of *a* axis of cation substituted $LiFe_{0.48}Mn_{0.48}Mg_{0.04}PO_4$ sample (the intermediate) lies between $LiFePO_4$ (PDF No. 01-070-6684) and $LiMnPO_4$ (PDF No. 77-0180) and the value of *b* axis is near the lattice parameter of $MnPO_4$ phase (PDF No. 07-0180). The value of *c* axis is near the lattice parameter of $FePO_4$ phase (PDF No. 01-070-6685). It has shown that *phase 1* is similar to $LiFe_{0.5}Mn_{0.5}PO_4$ phase (PDF No. 00-047-0478) and *phase 3* is similar to

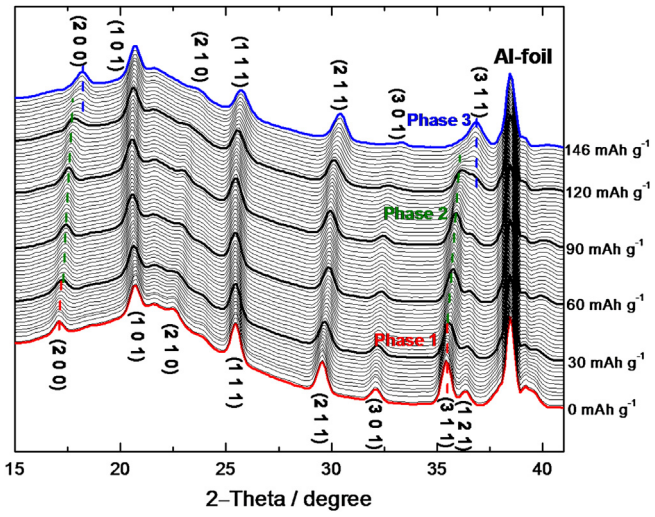

Fig. 4. The *in situ* XRD patterns of $LiFe_{0.48}Mn_{0.48}Mg_{0.04}PO_4$ during first charge.

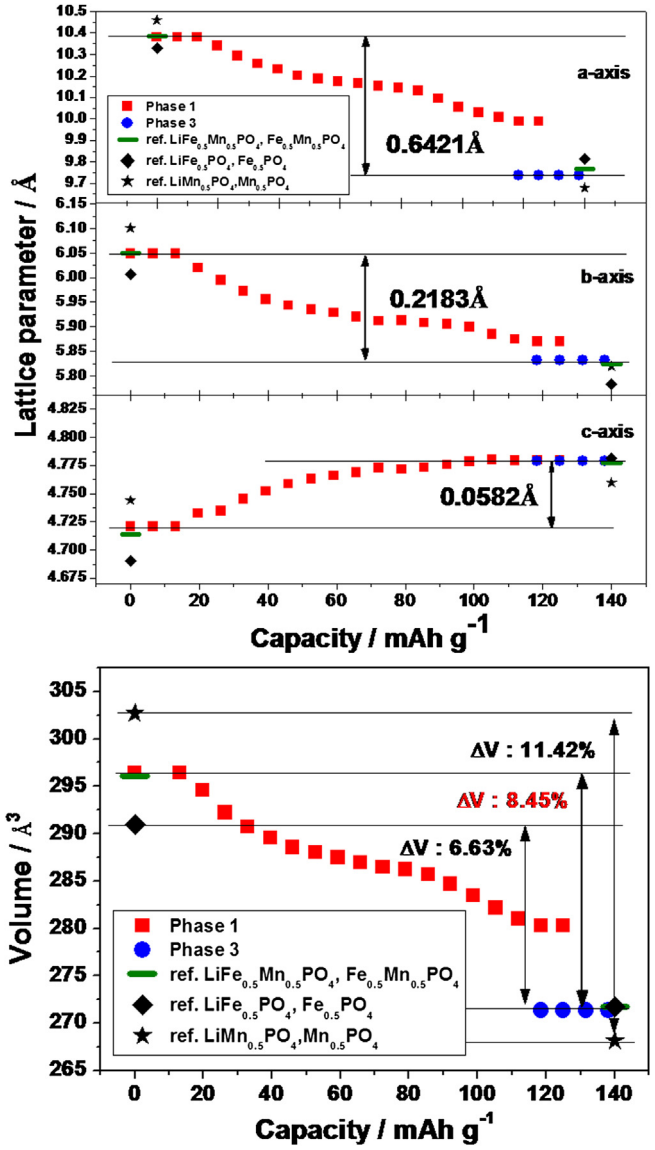

Fig. 5. Lattice parameters and unit-cell volumes of $LiFe_{0.48}Mn_{0.48}Mg_{0.04}PO_4$ cathode material and reference compounds.

$Fe_{0.5}Mn_{0.5}PO_4$ phase (PDF No. 01-073-7355). Lattice shrinkage takes place when it proceeds the reaction from *phase 1*($V = 296.41$ Å^3) to *phase 3* ($V = 271.35$ Å^3) resulting in global volume shrinkage of about 8.45% ($\Delta V = 25.06$ Å^3) during charge.

Cation substitution induces the shrinkage of crystal lattice due to the smaller ionic radius of Mg^{2+} ions ($Mn^{2+} > Fe^{2+} > Mg^{2+} > Mn^{3+} > Fe^{3+}$) [16–19]. Lattice distortion is more pronouncing when materials have Jahn–Teller-active ions. Meethong et al. have reported that crystalline misfit at the phase boundary between $LiMnPO_4$ and $MnPO_4$ is larger than the misfit created between $LiFePO_4$ and $FePO_4$ due to Jahn–Teller-active Mn^{3+} ions [19]. When Li ions are removed electrochemically from the above system, remaining framework has the same *Pnma* symmetry with 6.6% of volume reduction. A smaller change in lattice parameter during Li extraction of $LiFe_{0.48}Mn_{0.48}Mg_{0.04}PO_4$ material favors the lithium ion diffusion in bulk structure. Crystalline misfit at the phase boundary between $LiMnPO_4$ and $MnPO_4$ (ca. 11.42% volume difference) is larger than the misfit created at the boundary between $LiFe_{0.48}Mn_{0.48}Mg_{0.04}PO_4$ and $Fe_{0.48}Mn_{0.48}Mg_{0.04}PO_4$ (ca. 8.45% difference). The smaller lattice mismatch creates a more favorable phase boundary facilitating the conversion of one phase to another resulting in less polarization and better rate capability of the material. This clearly demonstrates that cation substitution of Mg^{2+} improves the kinetics of multi-component Fe–Mn based olivine structure cathode materials. Cation substitution finds a way to mitigate the lattice distortion and decreases the misfits near the phase boundary.

4. Conclusions

We have investigated the local and bulk structure of $LiFe_{0.48}Mn_{0.48}Mg_{0.04}PO_4$ system by using *in situ* XAS and XRD. From Fe and Mn K-edge XANES results, it was concluded that the major charge compensation at the metal site during charge is achieved by the oxidation of Fe^{2+} ions at a lower potential plateau (~3.5 V) and the oxidation of Mn^{2+} ions at a higher potential plateau (~4.1 V). From the peak changes of first coordination shell of Fe K-edge EXAFS spectra, it was confirmed that Mg^{2+} substitution causes smaller local structure distortion and disorder during lithium extraction. XAS study revealed that atoms around Fe ions are well ordered and it is consistent with the phase change mechanism and formation of pseudo one phase reaction from *in situ* XRD result. Substitution of Mg^{2+} ion induces change in lattice parameter and also decreases the lattice mismatch near the phase boundary between $LiFe_{0.48}Mn_{0.48}Mg_{0.04}PO_4$ and $Fe_{0.48}Mn_{0.48}Mg_{0.04}PO_4$ improving the reaction kinetics and rate capability of electrode.

Acknowledgments

This work was supported by the National Research Foundation funded by the Korean Government (MEST: NRF-2010-0029065) and the Human Resources Development program (No. 20124010203270) of KETEP funded by the Korean government Ministry of Knowledge Economy.

References

[1] A.K. Padhi, K.S. Nanjundaswamy, J.B. Goodenough, J. Electrochem. Soc. 144 (1997) 1188–1194.
[2] N.N. Bramnik, K.G. Bramnik, K. Nikolowski, M. Hinterstein, C. Baehtz, H. Ehrenberg, Electrochem. Solid-State Lett. 8 (2005) A379–A381.
[3] G. Li, Y. Kudo, K.-Y. Liu, H. Azuma, M. Tohda, J. Electrochem. Soc. 149 (2002) A1414–A1418.
[4] K.-W. Nam, W.-S. Yoon, K. Zaghib, K. Yoon Chung, X.-Q. Yang, Electrochem. Commun. 11 (2009) 2023–2026.
[5] A. Yamada, Y. Kudo, K.-Y. Liu, J. Electrochem. Soc. 148 (2001) A747–A754.

[6] G. Chen, J.D. Wilcox, T.J. Richardson, Electrochem. Solid-State Lett. 11 (2008) A190–A194.
[7] A. Yamada, Y. Kudo, K.-Y. Liu, J. Electrochem. Soc. 148 (2001) A1153–A1158.
[8] Y.Z. Dong, Y.M. Zhao, H. Duan, Mater. Chem. Phys. 129 (2011) 756–760.
[9] G. Hautier, A. Jain, S.P. Ong, B. Kang, C. Moore, R. Doe, G. Ceder, Chem. Mater. 23 (2011) 3495–3508.
[10] H. Fang, E. Dai, B. Yang, Y. Yao, W. Ma, J. Power Sources 204 (2012) 193–196.
[11] J.-W. Lee, M.-S. Park, B. Anass, J.-H. Park, M.-S. Paik, S.-G. Doo, Electrochim. Acta 55 (2010) 4162–4169.
[12] K.-W. Nam, X.-J. Wang, W.-S. Yoon, H. Li, X. Huang, O. Haas, J. Bai, X.-Q. Yang, Electrochem. Commun. 11 (2009) 913–916.
[13] M. Balasubramanian, X. Sun, X.Q. Yang, J. McBreen, J. Power Sources 92 (2001) 1–8.
[14] A. Deb, U. Bergmann, E.J. Cairns, S.P. Cramer, J. Phys. Chem. B 108 (2004) 7046–7051.
[15] T. Nedoseykina, M.G. Kim, S.-A. Park, H.-S. Kim, S.-B. Kim, J. Cho, Y. Lee, Electrochim. Acta 55 (2010) 8876–8882.
[16] W. Yoon, K. Chung, J. McBreen, K. Zaghib, X. Yang, Electrochem. Solid-State Lett. 9 (2006) A415–A417.
[17] G. Kobayashi, S.-i. Nishimura, M.-S. Park, R. Kanno, M. Yashima, T. Ida, A. Yamada, Adv. Funct. Mater. 19 (2009) 395–403.
[18] X. Ou, G. Liang, L. Wang, S. Xu, X. Zhao, J. Power Sources 184 (2008) 543–547.
[19] N. Meethong, H.-Y.S. Huang, W.C. Carter, Y.-M. Chiang, Electrochem. Solid-State Lett. 10 (2007) A134–A138.